






# Thioredoxin-interacting protein is essential for memory T cell formation via the regulation of the redox metabolism

Kota Kokubo<sup>a,1</sup> , Kiyoshi Hirahara<sup>a,1,2</sup> , Masahiro Kiuchi<sup>a,1</sup>, Kaori Tsuji<sup>a</sup>, Yuki Shimada<sup>a</sup>, Yuri Sonobe<sup>a</sup>, Rie Shinmi<sup>a</sup>, Takahisa Hishiya<sup>a</sup>, Chiaki Iwamura<sup>a</sup>, Atsushi Onodera<sup>a,b</sup>, and Toshinori Nakayama<sup>a,c,2</sup> 

Edited by Jeff Rathmell, Vanderbilt University Medical Center, Nashville, TN; received October 27, 2022; accepted November 30, 2022 by Editorial Board Member Philippa Marrack

CD4<sup>+</sup> memory T cells are central to long-lasting protective immunity and are involved in shaping the pathophysiology of chronic inflammation. While metabolic reprogramming is critical for the generation of memory T cells, the mechanisms controlling the redox metabolism in memory T cell formation remain unclear. We found that reactive oxygen species (ROS) metabolism changed dramatically in T helper-2 (Th2) cells during the contraction phase in the process of memory T cell formation. Thioredoxin-interacting protein (Txnip), a regulator of oxidoreductase, regulated apoptosis by scavenging ROS via the nuclear factor erythroid 2-related factor 2 (Nrf2)–biliverdin reductase B (Blvrb) pathway. Txnip regulated the pathology of chronic airway inflammation in the lung by controlling the generation of allergen-specific pathogenic memory Th2 cells in vivo. Thus, the Txnip–Nrf2–Blvrb axis directs ROS metabolic reprogramming in Th2 cells and is a potential therapeutic target for intractable chronic inflammatory diseases.

thioredoxin-interacting protein (Txnip) | reactive oxygen species (ROS) | nuclear factor-erythroid factor 2-related factor 2 (Nrf2) | biliverdin reductase B (Blvrb) | memory Th2 cells

CD4<sup>+</sup> memory T cells are central to adaptive immunity and play a critical role in the host defense against microorganisms (1). CD4<sup>+</sup> memory T cells are also involved in shaping the pathology of chronic inflammation (2). Upon antigen recognition by T cell receptor (TCR), naïve CD4<sup>+</sup> T cells proliferate and differentiate into effector T cells. After elimination of antigens, most of the effector T cells die by apoptosis in the contraction phase (3), but some survive and become long-lived memory T cells. The population size of the antigen-specific memory T cells is important for ensuring quality adaptive immune responses (4, 5). Metabolic reprogramming, including the upregulation of adenosine monophosphate-activated protein kinase signaling and downregulation of mechanistic target of rapamycin signaling in T cells, is crucial for the formation of antigen-specific memory T cells (6, 7). However, metabolic reprogramming in other pathways, such as reactive oxygen species (ROS) metabolism, which regulates the formation of memory T cells, remains unclear.

Metabolic reprogramming is also known to be essential for the proper activation of naïve T cells and their differentiation into effector T cells (8–10). Antigen stimulation via TCR causes a dramatic increase in aerobic glycolysis, which induces the generation of ROS in effector T cells (11, 12). ROS are also produced in mitochondria during the metabolic process of oxidative phosphorylation or by NADPH oxidase expressed in effector T cells (13–15). ROS are necessary for the transmission of TCR signaling and subsequent proliferation of effector T cells during the expansion phase (14). However, they also induce activation-induced apoptotic cell death of effector T cells via DNA damage and the outflow of cytochrome C via depolarization of the mitochondrial membrane (16, 17). Thus, the appropriate regulation of cellular ROS metabolism is required to ensure proper differentiation of effector T cells. However, the role of ROS metabolism in the formation of memory T cells remains unclear.

In the present study, we investigated the changes in ROS metabolism and its regulation of the formation of CD4<sup>+</sup> memory T cells. We found that ROS metabolism dramatically shifts from the production to the scavenging of effector T cells during the contraction phase. The thioredoxin-binding protein Txnip was gradually up-regulated in effector T cells during the contraction phase. It scavenged cellular ROS by activating the Nrf2–Blvrb pathway but not by activating thioredoxin in effector T cells. Furthermore, we found that Txnip regulated the pathology of allergic airway inflammation in the lung by controlling the number of antigen-specific memory T helper-2 (Th2) cells in vivo. Thus, metabolic shift from ROS production to ROS scavenging via the Txnip–Nrf2–Blvrb pathway is essential for the formation of the memory-type pathogenic Th2 cells that shape the pathology of allergic inflammation.

## Significance

Metabolic reprogramming is crucial for the generation of memory T cells; however, the mechanisms that control the redox metabolism in allergen-specific memory T cell formation still remain unclear. In this study, we found that thioredoxin-interacting protein (Txnip), a regulator of oxidoreductase, controlled reactive oxygen species (ROS) metabolism via the nuclear factor erythroid 2-related factor 2 (Nrf2)–biliverdin reductase B (Blvrb) pathway, which made memory Th2 cell generation possible and shaped the pathology of allergic airway inflammation. This study will contribute to the development of therapeutic strategies for intractable inflammatory diseases by focusing on the redox metabolism and the formation of CD4<sup>+</sup> memory T cells.

Author contributions: K.K., K.H., M.K., and C.I. designed research; K.K., K.H., M.K., K.T., Y. Shimada, Y. Sonobe, R.S., and T.H. performed research; K.K., K.H., M.K., A.O., and T.N. analyzed data; and K.K., K.H., and T.N. wrote the paper.

The authors declare no competing interest.

This article is a PNAS Direct Submission. J.R. is a guest editor invited by the Editorial Board.

Copyright © 2023 the Author(s). Published by PNAS. This article is distributed under [Creative Commons Attribution-NonCommercial-NoDerivatives License 4.0 \(CC BY-NC-ND\)](https://creativecommons.org/licenses/by-nc-nd/4.0/).

<sup>1</sup>K.K., K.H., and M.K. contributed equally to this work.

<sup>2</sup>To whom correspondence may be addressed: hiraharak@chiba-u.jp or tnakayama@faculty.chiba-u.jp.

This article contains supporting information online at <https://www.pnas.org/lookup/suppl/doi:10.1073/pnas.2218345120/-/DCSupplemental>.

Published January 3, 2023.

## Results

**The Metabolic Pathways for Scavenging Oxidative Stress Were Up-Regulated in CD4<sup>+</sup> T Cells during the Contraction Phase In Vivo.** To determine the dynamics of cellular ROS in CD4<sup>+</sup> T cells, we first examined the intensity of CellROX, an oxidative stress reagent that is nonfluorescent in a reduced state and exhibits intense fluorogenic signal upon oxidation, in naïve, effector, and memory CD4<sup>+</sup> T cells (*SI Appendix, Fig. S1 A and B*). Effector Th2 cells showed a higher fluorescence intensity of CellROX signals than that in naïve CD4<sup>+</sup> T or memory Th2 cells (Fig. 1 *A and B*). A fluorescence-activated cell sorting analysis confirmed the increase in the mean fluorescence intensity (MFI) of CellROX in effector Th2 cells (Fig. 1 *C and D* and *SI Appendix, Fig. S1 C and D*).

To assess the dynamics of cellular ROS in more detail, we performed an in vivo experiment, in which OVA-specific naïve CD4<sup>+</sup> T cells were adoptively transferred to syngeneic BALB/c mice that had been administered ovalbumin (OVA) and Alum intraperitoneally on days 1 and 6 (*SI Appendix, Fig. S1E*). The cell number and MFI of CellROX in antigen-specific CD4<sup>+</sup> T cells started to decrease between 7 and 11 d after the initial antigen administration, followed by a gradual decrease up to 2 mo in vivo (*SI Appendix, Fig. S1E* and Fig. 1*E*). These results indicate that antigen-reactive CD4<sup>+</sup> T cells on days 7 and 11 were in the effector and contraction phases, respectively. In another experimental model in which in vitro-differentiated effector CD4<sup>+</sup> T cells were adoptively transferred, a significant decrease in the MFI of CellROX was also observed at 48 h after cell transfer (*SI Appendix, Fig. S1 F and G*).

We next performed single-cell RNA sequencing (scRNA-Seq) using cells at 7 and 11 d after the initial antigen administration (Fig. 1*F*). A single-sample Gene set variation analysis (ssGSVA) revealed that the metabolic pathways related to the scavenging oxidative stress, including the “oxidation–reduction process” and “oxidoreductase activity” pathways, were enriched in cells at 11 d compared to those at 7 d after the initial antigen administration (Fig. 1 *G and H*); furthermore, these pathways were also enriched in transferred Th2 cells that had been collected 48 h after adoptive transfer (*SI Appendix, Fig. S1 H–J*). Thus, the levels of cellular ROS in CD4<sup>+</sup> T cells in the contraction phase were dramatically decreased, accompanied by an increased expression of genes involved in scavenging oxidative stress.

**The Thioredoxin-Interacting Protein Txnip Is Up-Regulated in the Contraction Phase.** A pseudo-time trajectory analysis revealed the differentiation trajectories of individual CD4<sup>+</sup> T cells recovered from mice 7 and 11 d after the initial antigen administration (Fig. 2*A*). Based on the differentiation trajectories determined by the pseudo-time, the genes were categorized into three major groups using Pearson’s correlation coefficient (Fig. 2*B*). Group 1 genes, including *Myc* and *Rtc4*, showed an apparent decrease in expression during the contraction phase (Fig. 2*C*, top rows [blue]). In sharp contrast, Group 3 genes, such as *Txnip* and *Foxp1*, showed an apparent increase in expression during the contraction phase (Fig. 2*C*, bottom rows [red]). Group 2 genes showed a gradual decrease in expression (Fig. 2*C*, middle rows [orange]). The uniform manifold approximation and projection (UMAP) analysis also revealed a similar expression pattern of representative genes among Groups 1, 2, and 3 (Fig. 2*D*).

Most of the 102 oxidative stress-related genes involved in the “oxidation–reduction process” or “oxidoreductase activity” pathways shown in Fig. 1*G* were up-regulated in antigen-reactive CD4<sup>+</sup> T cells 11 d after the initial antigen administration (Fig. 2*E* orange color dots). *Txnip*, which encodes thioredoxin-interacting protein, showed the highest fold expression among the

up-regulated oxidative stress-related genes in antigen-reactive CD4<sup>+</sup> T cells 11 d after the initial antigen administration (Fig. 2*E* and *SI Appendix, Fig. S2A*). *Txnip* also showed the highest fold change in expression between transferred Th2 cells that were recovered from mice 48 h after adoptive transfer and effector Th2 cells among all the up-regulated oxidative stress-related genes (*SI Appendix, Fig. S2 B–H*). Thus, the majority of the oxidative stress-related genes, including *Txnip*, were up-regulated in the CD4<sup>+</sup> T cells during the contraction phase in vivo.

***Txnip* Deficiency Resulted in Enhanced Apoptosis Accompanied by an Increased MFI of CellROX in Transferred Th2 Cells.** We next investigated the role of *Txnip* in CD4<sup>+</sup> T cells using genetically modified mice. CD4-specific *Txnip*-deficient mice (referred *Txnip* KO mice from now on) at 6 to 12 wk old showed a comparable proportion of CD4<sup>+</sup> T cells in the thymus and spleen to control wild-type mice, consistent with a previous report (18) (*SI Appendix, Fig. S3 A–D*). *Txnip*-deficient effector T cells, including Th1, Th2, and Th0 cells, produced a similar amount of effector cytokines to wild-type effector T cells (*SI Appendix, Fig. S3E*).

At 48 h after adoptive transfer (*SI Appendix, Fig. S3F*), *Txnip*-deficient transferred Th2 cells showed a higher MFI of CellROX than wild-type Th2 cells (Fig. 3 *A, Right*), although *Txnip*-deficient effector Th2 cells showed a comparable MFI of CellROX to wild-type effector Th2 cells (Fig. 3 *A, Left*). In whole cells, *Txnip* deficiency in transferred Th2 cells resulted in an increased percentage of annexin V-positive cells and a decreased number of cells compared with wild-type cells (Fig. 3 *B and C* and *SI Appendix, Fig. S3 G–J*). The administration of MitoTEMPO and Trolox, ROS scavenger reagents that have been reported to quench ROS and oxidative damage in vivo (19, 20), inhibited the elevation of the MFI of CellROX in *Txnip*-deficient transferred Th2 cells (Fig. 3 *D and E, Left*). The administration of these ROS scavenger reagents also inhibited the elevation of annexin V-positive cells in *Txnip*-deficient transferred Th2 cells (Fig. 3 *D and E, Middle and Right*). Preloading with methyl-GSH, another ROS scavenger reagent (21), resulted in decreased ROS levels in both *Txnip*-deficient effector and transferred Th2 cells (*SI Appendix, Fig. S3 K and L, Left*). However, the preloading of methyl-GSH showed relatively little effect on apoptosis in *Txnip*-deficient transferred Th2 cells (*SI Appendix, Fig. S3 L, Middle and Right*). Thus, *Txnip* deficiency resulted in an increased MFI of CellROX and increased apoptosis in transferred Th2 cells.

Thioredoxin, a ROS scavenging oxidoreductase, is a binding partner of *Txnip* (22). *Txnip* restrains the oxidoreductive function of thioredoxin through its binding (23). Unexpectedly, *Txnip*-deficient transferred Th2 cells showed no marked difference in the protein expression of thioredoxin (*SI Appendix, Fig. S3 M and N*) or thioredoxin activity (*SI Appendix, Fig. S3O*) from wild-type effector or transferred Th2 cells. To explore the molecular mechanisms underlying the ROS scavenging by *Txnip* in transferred Th2 cells, we performed scRNA-Seq analyses using wild-type or *Txnip*-deficient Th2 cells recovered 48 h after cell transfer. Characteristic clusters of *Txnip*-deficient Th2 cells were detected among transferred Th2 cells but not among effector Th2 cells (Fig. 3*F* and *SI Appendix, Fig. S3P*). Nuclear factor-erythroid factor 2-related factor 2 (Nrf2) is a transcription factor that regulates scavenging oxidative stress (24). The ssGSVA analysis showed that the Nrf2-downstream pathways, including “Nrf2-ARE PATHWAY” and “Nrf2-ARE REGULATION,” were enriched in wild-type compared with *Txnip*-deficient transferred Th2 cells (Fig. 3*G*). In both pathways, the GSVA score was decreased in *Txnip*-deficient transferred Th2 cells compared with wild-type transferred Th2 cells (Fig. 3*H*). Consistent with these results, the

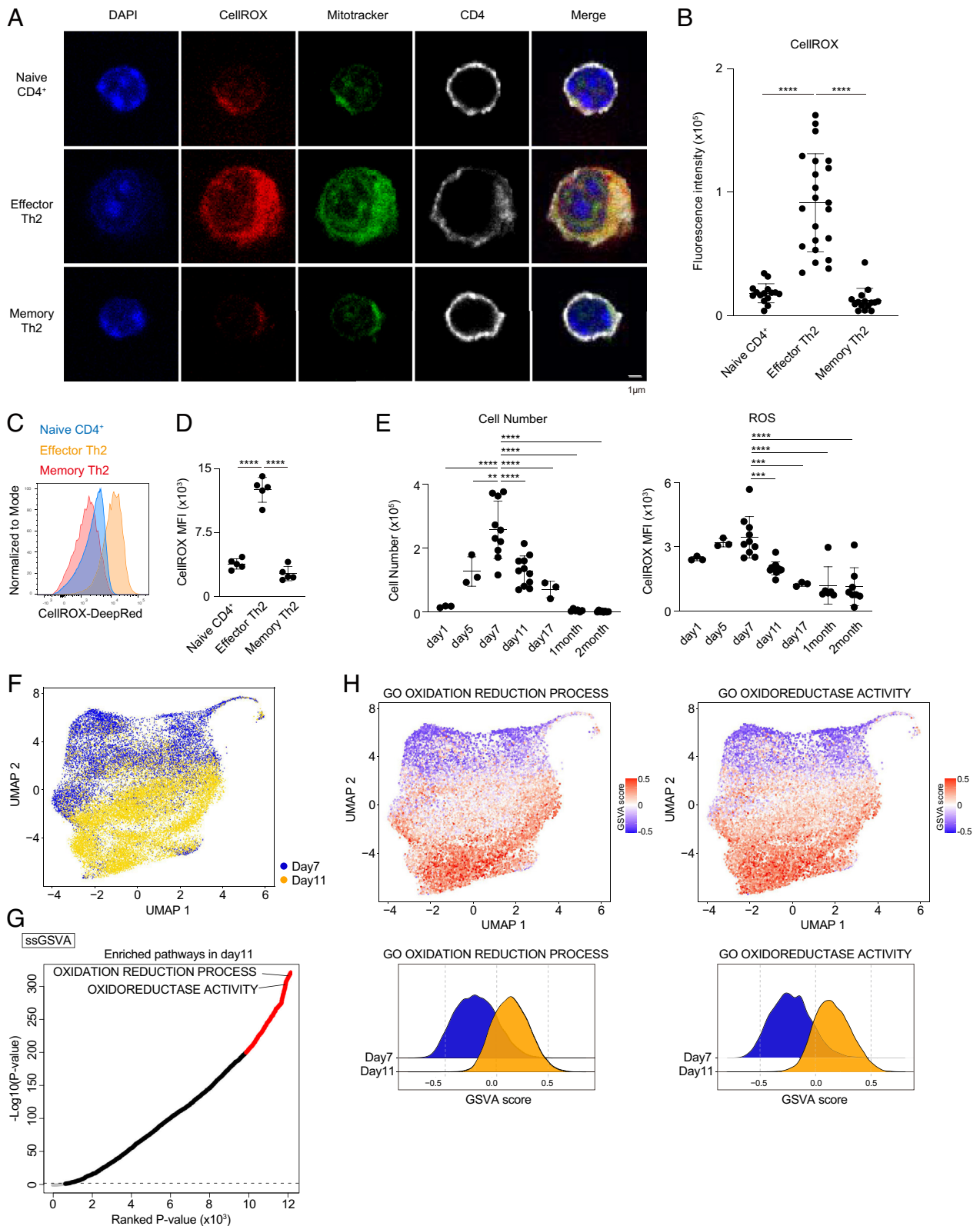


**Fig. 1.** Pathways for scavenging oxidative stress are activated in CD4<sup>+</sup> T cells during the contraction phase in vivo. (A) Representative confocal micrograph images of naïve CD4<sup>+</sup> T cells, effector Th2 cells, and memory Th2 cells stained with DAPI (blue), CellROX (red), Mitotracker (green), and anti-CD4 (white). The white bar in the image is a 1-μm scale bar. Representative findings of two independent experiments are shown. (B) Fluorescence intensities of CellROX in each cell are shown (naïve CD4<sup>+</sup> and memory Th2, n=15; effector Th2, n=22). (C and D) A representative histogram plot (C) and the MFI (D) of CellROX from two independent experiments are shown (n=5). (E) The number (Left) and MFI of CellROX (Right) of transferred T cells at each time point after cell transfer (days 1, 5, and 17, n=3; day 7, n=10; day 11, n=11; 1 mo, n=6; 2 mo, n=8) from four independent experiments are shown. (F) A UMAP projection of transferred T cells at days 7 (blue) and 11 (orange) after cell transfer is depicted. (G) A ranking plot of ssGSVA scores is depicted. Red dots indicate the top 10% pathways. (H) ssGSVA scores of oxidation-reduction process (left column) and oxidoreductase activity (right column) are projected on UMAPs (upper row) and ridgeline plots (lower row). (F–H) Cells from two mice were pooled for each group. Data are expressed as the mean ± SD. P-values were calculated by a one-way ANOVA. \*\*P < 0.01, \*\*\*P < 0.001, \*\*\*\*P < 0.0001.

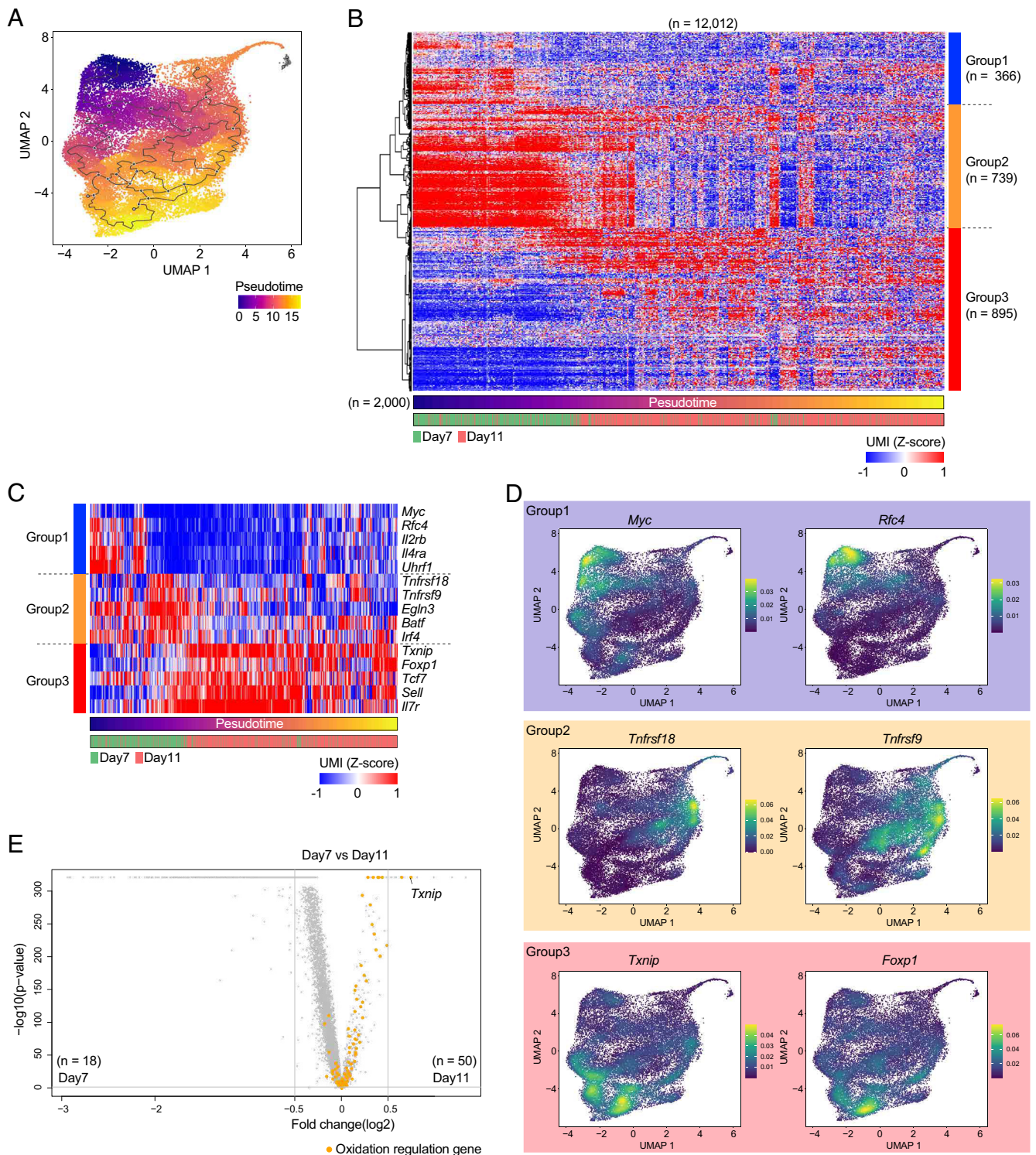


**Fig. 2.** Thioredoxin-interacting protein, Txnip is up-regulated in transferred T cells. (A–E) Analyses of scRNA-Seq data of transferred T cells at days 7 and 11 after cell transfer. A UMAP projection of transferred T cells at days 7 and 11 with the pseudo-time trajectory analysis is depicted (A). The plotting symbol for each cell is colored based on the pseudo-time. Cells that have infinite pseudo-time are shown in gray. The relative expression of genes (rows) across cells (columns) is shown (B). The cells sorted by pseudo-time are determined in Fig. 2A. The genes are classified into three groups based on the temporal expression patterns. A gene expression heat map of the top five characteristic genes in each group (Group 1, blue; Group 2, orange; and Group 3, red) is depicted (C). Density plots on UMAPs colored by the density of each cell in the expression of top two characteristic genes in each group (Group 1, upper row; Group 2, middle row; and Group 3, lower row) are shown (D). A volcano plot that shows the differential gene expression between transferred T cells at days 7 and 11 is depicted (E). Orange dots indicate the oxidative stress-related genes, which are included in the two pathways in Fig. 1H.

protein expression of Nrf2 was reduced in *Txnip*-deficient transferred Th2 cells (Fig. 3 I and J, and *SI Appendix*, Fig. S3Q). These results suggest that Txnip may activate Nrf2-downstream genes and scavenge cellular ROS in transferred Th2 cells via regulation of the protein expression of Nrf2.

**Txnip Regulates the Scavenging of Cellular ROS via the Nrf2-Blvrb Pathway.** We next performed conventional RNA-Seq analyses using transferred Th2 cells from wild-type and *Txnip* KO mice to determine the Nrf2-downstream genes. We noted the decreased expression of *Biliverdin reductase B* (*Bvlrb*), which

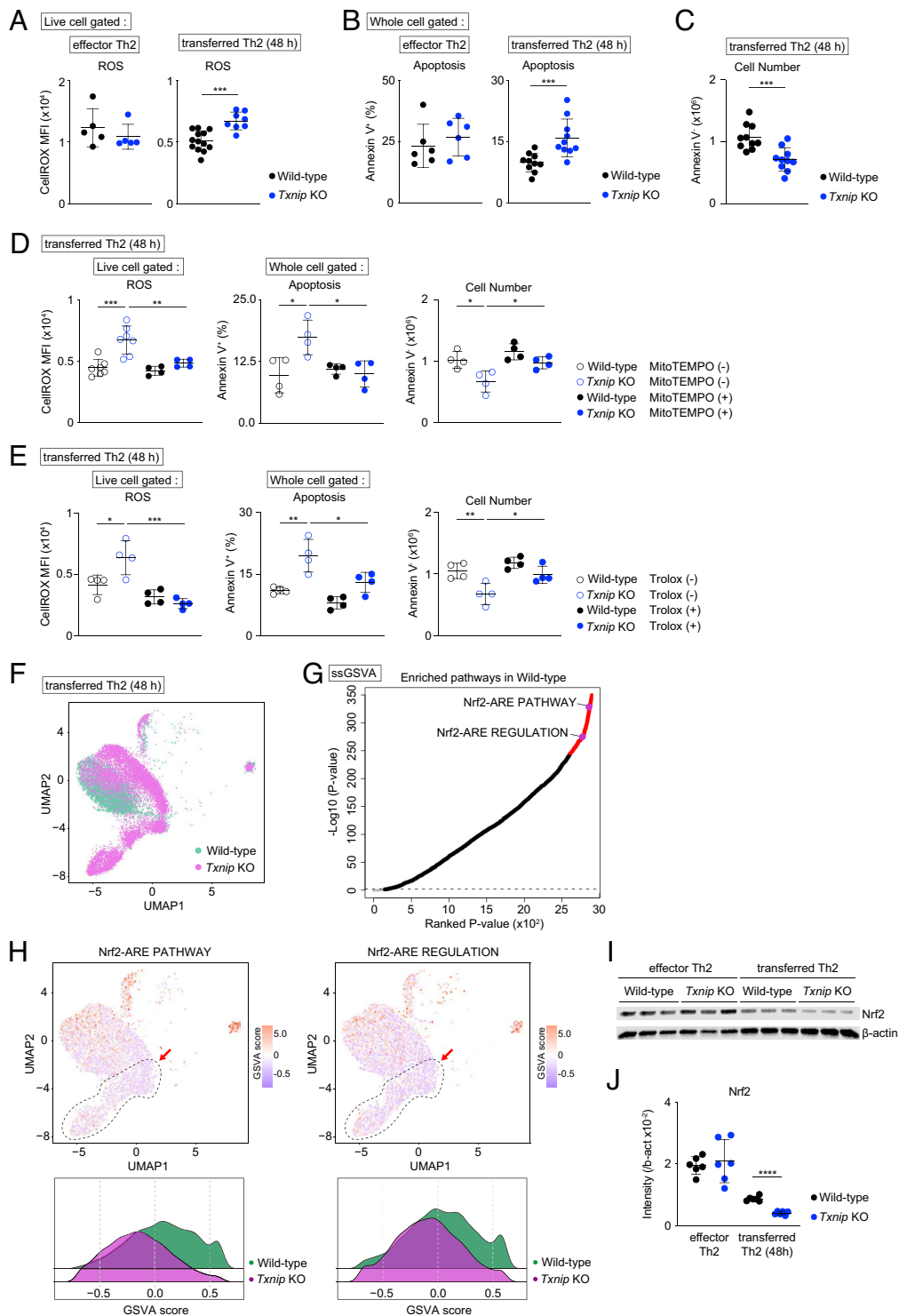


**Fig. 3.** *Txnip* deficiency causes enhanced apoptosis accompanied by increased cellular ROS in transferred Th2 cells. (A) The MFI of CellROX of wild-type or *Txnip*-deficient effector Th2 cells (Left panel; wild-type: n=5, *Txnip*-deficient: n=5) and transferred Th2 cells (Right panel; wild-type: n=13, *Txnip*-deficient: n=8) from more than two independent experiments are shown. (B) Percentages of annexin V<sup>+</sup> cells in effector Th2 cells (Left panel; wild-type: n=6, *Txnip*-deficient: n=6) and transferred Th2 cells (Right panel; wild-type: n=10, *Txnip*-deficient: n=10) from six independent experiments are shown. (C) The number of annexin V<sup>+</sup> cells in transferred Th2 cells. (D) The MFI of CellROX (Left panel; MitoTEMPO (-): n=7 in both wild-type and *Txnip*-deficient transferred Th2 cells, MitoTEMPO (+): n=4 in both wild-type and *Txnip*-deficient transferred Th2 cells), percentages of annexin V<sup>+</sup> cells (Middle panel; n=4 in all indicated groups), and the number of annexin V<sup>+</sup> cells (Right panel; n=4 in all indicated groups) in transferred Th2 cells with in vivo MitoTEMPO treatment. The data from three independent experiments are shown. (E) The MFI of CellROX (Left), percentages of annexin V<sup>+</sup> cells (Center), and the number of annexin V<sup>+</sup> cells (Right) in transferred Th2 cells with in vivo Trolox treatment (n=4 in all indicated groups). The data from two independent experiments are shown. (F–H) Analyses of scRNA-Seq data of wild-type and *Txnip*-deficient transferred Th2 cells. A UMAP projection of wild-type (green) and *Txnip*-deficient (purple) transferred Th2 cells is depicted (F). A ranking plot of ssGSVA scores is depicted. Red dots indicate the top 10% pathways (G). ssGSVA scores of NRF2-ARE PATHWAY (left column) and NRF2-ARE REGULATION (right column) are projected on UMAPs (upper row) and ridgeline plots (lower row) (H). The dotted line with the red arrow indicates *Txnip*-deficient Th2 cell-specific cell population. Cells from two mice were pooled for each group (F–H). (I and J) An immunoblot analysis of the Nrf2 expression from two independent experiments. A representative immunoblot is shown in I.  $\beta$ -actin was used as a loading control. Quantified intensities of Nrf2 are shown in J (n=6 in all indicated groups). Data are expressed as the mean  $\pm$  SD. *P*-values were calculated by the Mann–Whitney *U* test (A–C, and J) and a one-way ANOVA (D and E). \**P* < 0.05, \*\**P* < 0.01, \*\*\**P* < 0.001, \*\*\*\**P* < 0.0001.

is a reductase and a downstream gene of Nrf2, in *Txnip*-deficient transferred Th2 cells (Fig. 4A and *SI Appendix, Fig. S4A*). A decreased number of *Blvrb*-expressing Th2 cells among *Txnip*-deficient cells was also detected in our scRNA-Seq data set (Fig. 4B). An assay to detect transposase-accessible chromatin using sequencing (ATAC-Seq) with transferred Th2 cells revealed the *Txnip*-dependent chromatin regulation in the *Blvrb* gene locus (Fig. 4C and *SI Appendix, Fig. S4B*). The protein expression of *Blvrb* was also reduced in *Txnip*-deficient transferred Th2 cells (Fig. 4D and E, and *SI Appendix, Fig. S4C*). Consistent with these results, the reductase activity of *Blvrb* was attenuated in *Txnip*-deficient transferred Th2 cells (Fig. 4F, *Right*) but not in *Txnip*-deficient effector Th2 cells (Fig. 4F, *Left*).

*Blvrb* mediates reduction of biliverdin to bilirubin and functions as a potent antioxidant through scavenging ROS (*SI Appendix, Fig. S4D*). The *Blvrb*-dependent reduction is driven by the cofactor nicotinamide adenine dinucleotide phosphate (NADPH) (25) (*SI Appendix, Fig. S4D*). We wondered whether or not the decreased activity of *Blvrb* in *Txnip*-deficient transferred Th2 cells was compensated by an increased production of NADPH. We found that the amount of NADPH was decreased in *Txnip*-deficient transferred Th2 cells (Fig. 4G and *SI Appendix, Fig. S4E*). At the same time, *Txnip* deficiency showed little effect on the uptake of glucose, fatty acids, or glutamine in transferred Th2 cells (*SI Appendix, Fig. S4F–I*). Finally, we found that the overexpression of the *Nfe2l2* gene, which encodes Nrf2, restored the expression of *Blvrb* significantly in *Txnip*-deficient transferred Th2 cells (Fig. 4H). Furthermore, the overexpression of *Nfe2l2* resulted in a decreased MFI of CellROX and decreased apoptosis in *Txnip*-deficient transferred Th2 cells (Fig. 4I and J). At the same time, the overexpression of *Blvrb* also resulted in a decreased MFI of CellROX and decreased apoptosis in *Txnip*-deficient transferred Th2 cells (Fig. 4K and L and *SI Appendix, Fig. S4J*). These results indicate that *Txnip* regulates the Nrf2–*Blvrb* pathway and controls the levels of cellular ROS and apoptotic cell death in Th2 cells.

#### ***Txnip* Deficiency Resulted in a Decreased Number of Memory Th2 Cells Accompanied by an Increased MFI of CellROX.**

Next, we explored whether or not *Txnip* was important for the proper formation of memory T cells in vivo. The expression of *Txnip* in Th2 cells after cell transfer increased over time (Fig. 5A). Even at 4 wk after adoptive transfer, *Txnip*-deficient cells showed a higher MFI of CellROX than wild-type Th2 cells (Fig. 5B). Furthermore, the numbers of *Txnip*-deficient transferred Th2 cells in vivo were consistently lower than those in wild-type transferred Th2 cells over 4 wk (Fig. 5C and D). The significant decrease in the number of *Txnip*-deficient transferred helper T cells in vivo was observed in not only Th2 cells but also Th1 and Th0 cells (*SI Appendix, Fig. S5A*). Moreover, 4 wk after adoptive transfer, an increased MFI of CellROX and decreased number of *Txnip*-deficient memory Th2 cells were observed in the lung, peripheral blood mononuclear cell (PBMC), bone marrow, and lymph nodes (Fig. 5E and F and *SI Appendix, Fig. S5B*). As expected, the overexpression of *Txnip* in effector Th2 cells resulted in an increased number of Th2 cells for at least 4 wk after cell transfer (Fig. 5G and H). Neither *Txnip* deficiency nor its overexpression showed any marked effect on the production of Th2 cytokines by memory Th2 cells, indicating that the Th2 cell function is not affected by the expression of *Txnip* (*SI Appendix, Fig. S5C and D*). Thus, *Txnip* regulates the levels of cellular ROS and the formation of memory Th2 cells in vivo while leaving their function intact.

#### ***Txnip* Regulates the Pathology of Allergic Airway Inflammation In Vivo.**

Finally, we investigated the roles of *Txnip* in the

formation of allergen-specific pathogenic memory Th2 cells that induce allergic airway inflammation in vivo. Wild-type mice and *Txnip* KO mice were administered OVA and HP- $\beta$ -CD adjuvant intranasally, and 5 wk later, they were challenged intranasally with OVA on days 42 and 43. Assays were performed on day 44 (Fig. 6A). The number of CD4<sup>+</sup>CD44<sup>hi</sup> memory T cells in the lung was significantly lower in OVA-challenged *Txnip* KO mice than those in OVA-challenged wild-type mice (Fig. 6B). Memory responses, such as infiltration of eosinophils in bronchoalveolar lavage fluid (BALF), were significantly decreased in *Txnip* KO mice along with decreased levels of Th2 cytokines, such as IL-4, IL-5, and IL-13 (Fig. 6C and D). Infiltration of inflammatory cells in the lung parenchyma was also decreased in *Txnip* KO mice (Fig. 6E). When *Txnip*-overexpressing OVA-specific (KJ1<sup>+</sup>) memory Th2 cells were transferred into recipient mice followed by challenge with OVA, the number of OVA-specific memory Th2 cells in the lung was significantly higher than those in control mice that had received mock-control Th2 cells (Fig. 6F and G). *Txnip* overexpression in memory Th2 cells resulted in enhanced memory responses, including increased infiltration of eosinophils (Fig. 6H), increased production of Th2 cytokines in BALF (Fig. 6I), and increased infiltration of inflammatory cells into the lung parenchyma (Fig. 6J). Thus, the pathology of allergic airway inflammation induced by allergen-specific memory Th2 cells was controlled by the expression of *Txnip* in CD4<sup>+</sup> T cells.

## **Discussion**

We identified *Txnip* as a key molecule in the regulation of ROS metabolism during the formation of allergen-specific memory Th2 cells that induce allergic airway inflammation in vivo. We found that cellular ROS metabolism dramatically shifted from the production process to the scavenging process in the contraction phase of Th2 cells. *Txnip*, as a ROS metabolism checkpoint molecule, scavenged cellular ROS via the activation of the Nrf2–*Blvrb* pathway. The genetic deletion of *Txnip* attenuated allergic airway inflammation as a result of the decreased formation of allergen-specific memory Th2 cells in vivo. In contrast, the overexpression of *Txnip* in Th2 cells exacerbated the pathology of airway inflammation due to the increased formation of allergen-specific memory Th2 cells. Thus, this study highlights unique molecular mechanisms in redox metabolism in Th2 cells that are crucial for the induction of allergen-specific memory responses in vivo.

Metabolic reprogramming during the activation of T cell is essential for inducing proper immune responses (9, 15). The ROS metabolism in CD4<sup>+</sup> T cells shifts to the production process to meet the energy requirements of activated CD4<sup>+</sup> T cells after TCR stimulation (14). ROS is required in order for activated CD4<sup>+</sup> T cells to produce IL-2 (26). The amount of cellular ROS is dramatically increased in effector T cells (17). We investigated the dynamics of cellular ROS once T cell activation had ceased and found a rapid decrease in cellular ROS in CD4<sup>+</sup> T cells during the contraction phase. This rapid decrease was probably induced by the enhanced scavenging pathways of cellular ROS. In CD8<sup>+</sup> T cells, CD28 signaling is reported to be critical for the downregulation of *Txnip*, which regulates mitochondrial fatty acid oxidation (27). Another group showed that TCR stimulation—rather than CD28 costimulation—was crucial for the downregulation of *Txnip* (18). In the current study, we found that *Txnip* was rapidly up-regulated once T cell activation ceased in CD4<sup>+</sup> T cells and that the upregulation of *Txnip* was critical for the formation of allergen-specific memory Th2 cells that induce allergic airway inflammation.

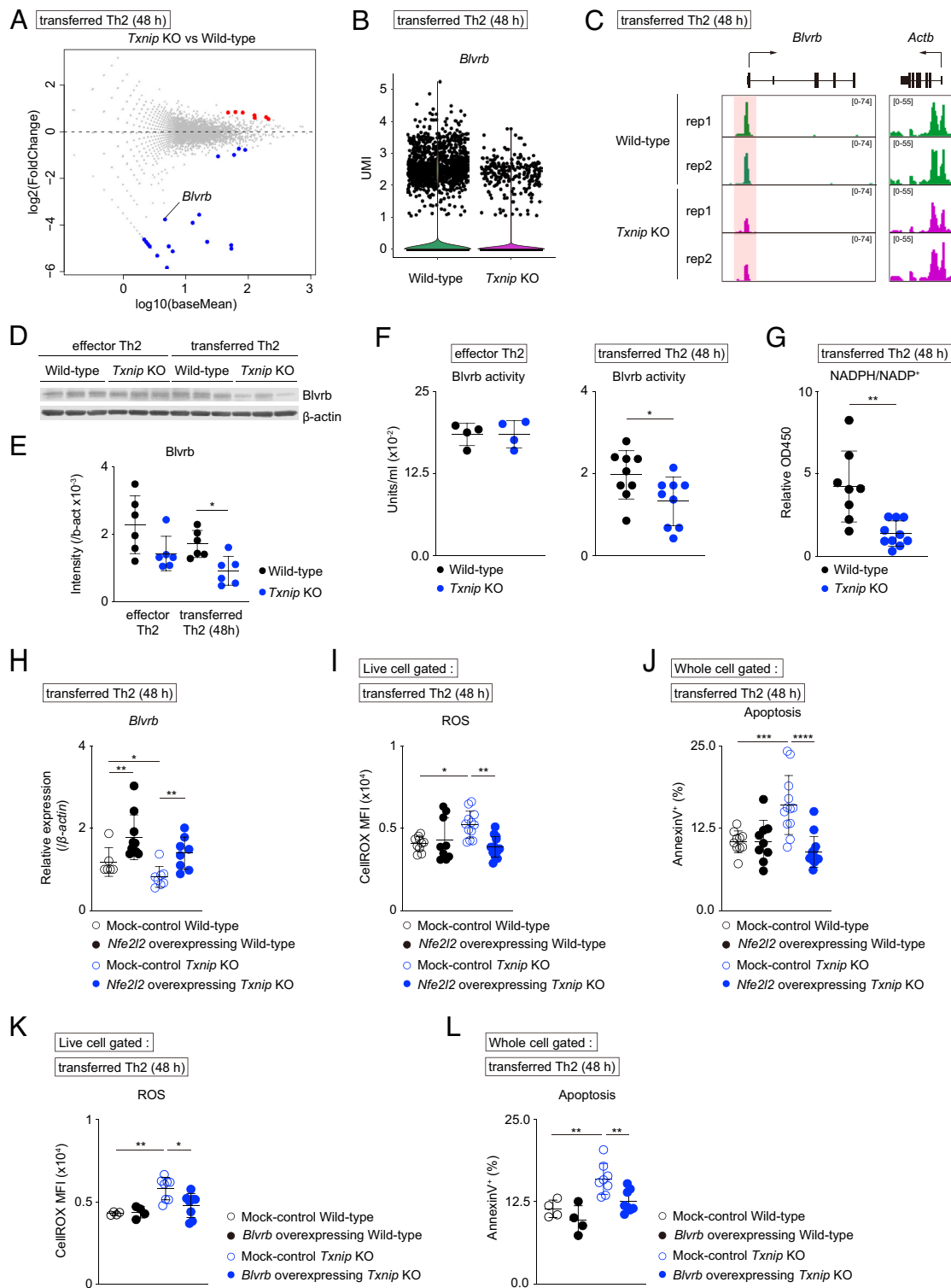


**Fig. 4.** *Txnip* regulates scavenging cellular ROS via the Nrf2–BlvrB pathway. (A) A MA plot for DESeq from the results of bulk RNA-Seq of wild-type and *Txnip*-deficient transferred Th2 cells is depicted. Colored dots indicate the genes that show fold changes >2 (red) or <1/2 (blue) accompanied by *P* values < 0.01. Three mice per group were analyzed. (B) Violin plots of *BlvrB* expression in wild-type and *Txnip*-deficient transferred Th2 cells are shown. (C) Gene track views of ATAC-Seq signals in wild-type transferred Th2 cells and *Txnip*-deficient transferred Th2 cells across the *BlvrB* gene locus and the *Actb* gene locus are shown. Two mice per group were analyzed. (D and E) An immunoblot analysis of the *BlvrB* expression from two independent experiments. A representative immunoblot is shown in D.  $\beta$ -actin was used as a loading control. Quantified intensities of *BlvrB* are shown in E ( $n=6$  in all indicated groups). (F) The *BlvrB* activity in effector Th2 cells (Left panel;  $n=4$  in both wild-type and *Txnip*-deficient effector Th2 cells) and transferred Th2 cells (Right panel;  $n=9$  in both wild-type and *Txnip*-deficient transferred Th2 cells) from two independent experiments is shown. (G) Ratios of the amount of NADPH to the amount of  $\text{NADP}^+$  in transferred Th2 cells (wild-type:  $n=8$ , *Txnip*-deficient:  $n=10$ ) from three independent experiments are shown. (H) The relative expression of *BlvrB* in transferred Th2 cells (mock-controlled wild-type:  $n=6$ , *Nfe2l2* overexpressing wild-type:  $n=10$ , mock-controlled *Txnip* KO:  $n=8$ , *Nfe2l2* overexpressing *Txnip*-deficient:  $n=8$ ) from four independent experiments is shown. (I and J) The MFI of CellROX (I) and percentages of annexin  $V^+$  cells (J) in transferred Th2 cells (mock-controlled wild-type:  $n=10$ , *Nfe2l2* overexpressing wild-type:  $n=9$ , mock-controlled *Txnip*-deficient:  $n=12$ , *Nfe2l2* overexpressing *Txnip*-deficient:  $n=13$ ) from six independent experiments are shown. (K and L) The MFI of CellROX (K) and percentages of annexin  $V^+$  cells (L) in transferred Th2 cells (mock-controlled or *BlvrB*-overexpressing wild-type:  $n=4$ , mock-controlled or *BlvrB*-overexpressing *Txnip*-deficient:  $n=8$ ) from two independent experiments are shown. Data are expressed as the mean  $\pm$  SD. *P*-values were calculated by Mann-Whitney *U* test (E–G, K, and L), or a one-way ANOVA (H–J). \**P* < 0.05, \*\**P* < 0.01, \*\*\**P* < 0.001, \*\*\*\**P* < 0.0001.

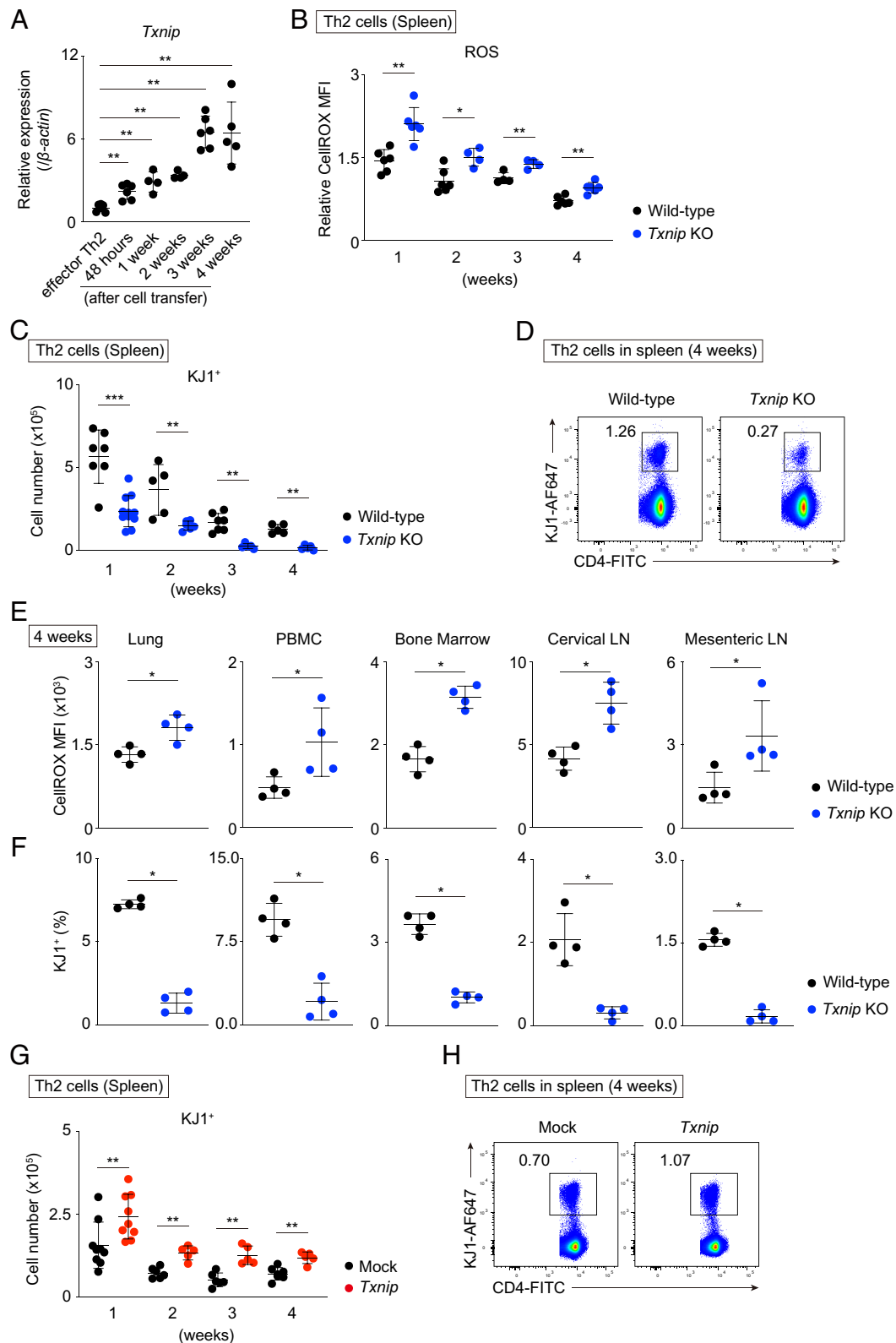


**Fig. 5.** Deletion of *Txnip* causes a decrease in the number of memory Th2 cells accompanied by an increased amount of ROS. (A) The relative expression of *Txnip* in the Th2 cells at each time point (effector Th2: n=6, 48 h: n=6, 1 wk: n=4, 2 wk: n=4, 3 wk: n=6, 4 wk: n=5) from three independent experiments is shown. (B and C) The relative MFI of CellROX, compared with naïve CD4<sup>+</sup> T cells (wild-type Th2 cells: n=6 in the indicated time point, *Txnip*-deficient Th2 cells; 1 wk: n=6, 2 wk: n=4, 3 wk: n=4, 4 wk: n=6) (B), and the number of transferred Th2 cells (wild-type Th2 cells; 1 wk: n=7, 2 wk: n=5, 3 wk: n=7, 4 wk: n=5, *Txnip*-deficient Th2 cells; 1 wk: n=11, 2 wk: n=6, 3 wk: n=5, 4 wk: n=5) (C) at each time point after cell transfer from more than three independent experiments are shown. (D) Representative plots of anti-CD4- and anti-OVA-specific TCR (KJ1) staining in spleen at 4 wk after cell transfer are shown. Three independent experiments were performed, with similar results. (E and F) MFI of CellROX of transferred Th2 cells (n=4 in each group) (E) and percentages of KJ1<sup>+</sup> cells in CD4<sup>+</sup> T cells (n=4 in each group) (F) recovered from each tissue at 4 wk after cell transfer from two independent experiments are shown. (G) The numbers of mock-control or *Txnip* overexpressing Th2 cells in spleens (mock; 1 wk: n=9, 2 wk: n=6, 3 wk: n=6, 4 wk: n=7, *Txnip* overexpression; 1 wk: n=9, 2 wk: n=5, 3 wk: n=5, 4 wk: n=5) from four independent experiments are shown. (H) Representative plots of cell surface staining of anti-CD4- and anti-OVA-specific TCR in transferred Th2 cells are shown. Three independent experiments were performed, with similar results. Data are expressed as the mean  $\pm$  SD. *P*-values were calculated by a one-way ANOVA (A), two-tailed unpaired *t* test (B), or Mann-Whitney *U* test (C, E, F, and G). \**P* < 0.05, \*\**P* < 0.01, \*\*\**P* < 0.001.



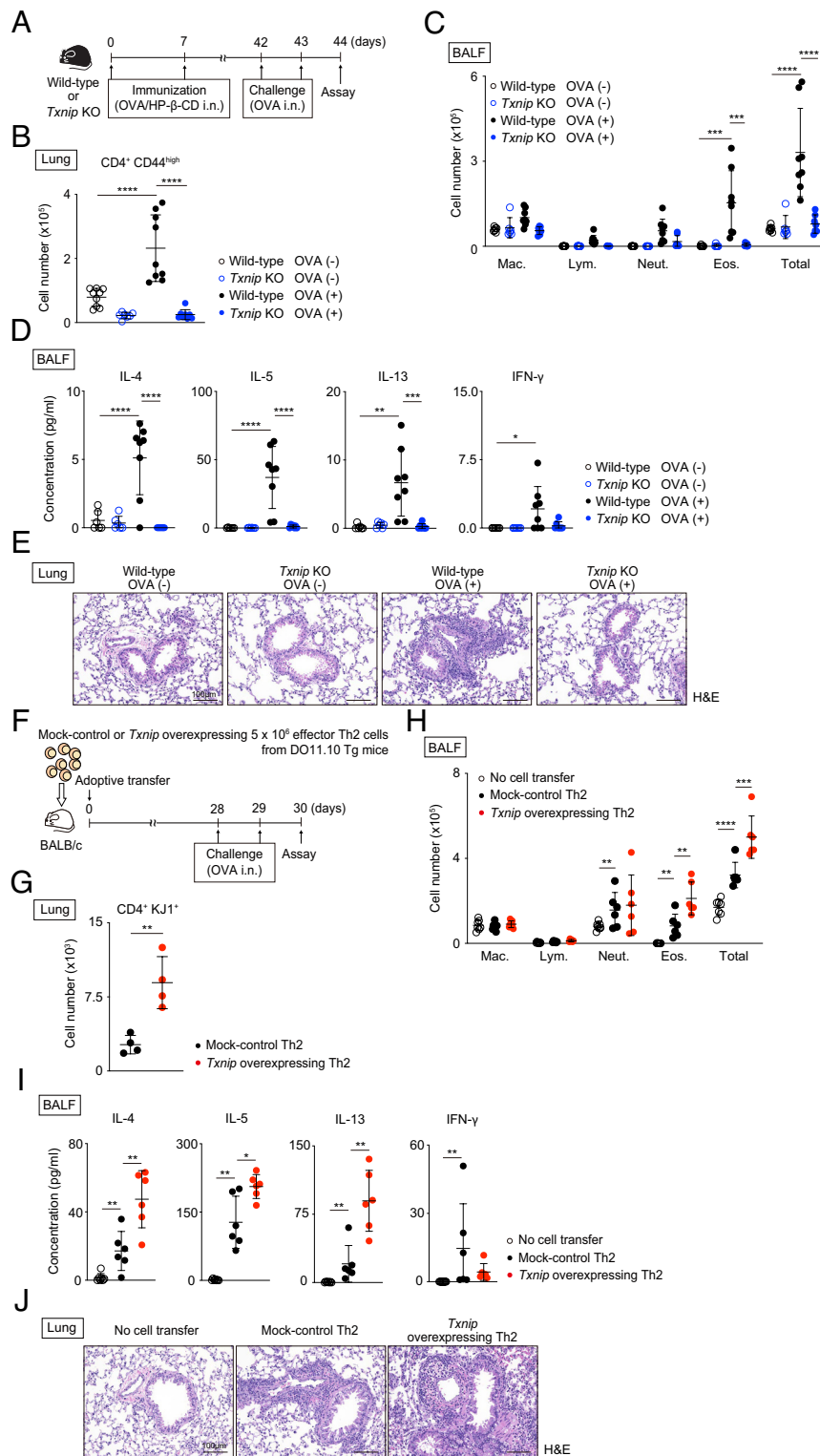


**Fig. 6.** Txnip regulates the pathology of allergic airway inflammation in vivo. (A) A schematic illustration of the intranasal exposure to OVA and HP- $\beta$ -CD followed by challenge with OVA after a 5-wk rest period is depicted. (B) The numbers of CD4<sup>+</sup>CD44<sup>high</sup> T cells recovered from the lungs (wild-type OVA (-): n=9, *Txnip* KO OVA (-): n=7, wild-type OVA (+): n=9, *Txnip* KO OVA (+): n=8) from two independent experiments are shown. (C and D) The numbers of macrophages (Mac.), lymphocytes (Lym.), neutrophils (Neut.), eosinophils (Eos.), and total cells (Total) (C) and the concentration of cytokines, including IL-4, IL-5, IL-13, and IFN- $\gamma$  (D) in BALF (wild-type OVA (-): n=6, *Txnip* KO OVA (-): n=6, wild-type OVA (+): n=8, *Txnip* KO OVA (+): n=7), from two independent experiments are shown. (E) Representative histological sections of the lungs stained with hematoxylin and eosin are shown. More than three mice per group were analyzed. Two independent experiments were performed, with similar results. (F) A schematic illustration of the intranasal exposure to OVA after a 4-wk rest period from the adoptive transfer is depicted. (G) The numbers of transferred Th2 cells recovered from the lungs in recipients of mock control or *Txnip* overexpressing Th2 cells (n=4 in each group) from two independent experiments are shown. (H and I) The numbers of macrophages, lymphocytes, neutrophils, eosinophils, and total cells (H) and the concentration of cytokines, including IL-4, IL-5, IL-13, and IFN- $\gamma$  (I) in BALF (mice without Th2 cell transfer: n=7, mice transferred with mock control Th2 cells: n=6, mice transferred with *Txnip* overexpressing Th2 cells: n=6), from two independent experiments are shown. (J) Representative histological sections of the lungs stained with hematoxylin and eosin are shown. More than three mice per group were analyzed. Two independent experiments were performed, with similar results. Data are expressed as the mean  $\pm$  SD. *P*-values were calculated by a one-way ANOVA (B and D), two-way ANOVA (C and H), or Mann-Whitney *U* test (G and I). \**P* < 0.05, \*\**P* < 0.01, \*\*\**P* < 0.001, \*\*\*\**P* < 0.0001.

The thioredoxin system, which is composed of NADPH, thioredoxin, and thioredoxin reductase, is important for the maintenance of cellular redox metabolism (28). The thioredoxin system scavenges cellular ROS through its disulfide reductase activity. Txnip binds to reduced thioredoxin and restrains the thioredoxin function (23). Importantly, however, we found that the thioredoxin activity was not changed in *Txnip*-deficient transferred Th2 cells. Instead, our single-cell RNA sequencing analysis revealed that a loss of Txnip resulted in the decreased activity of the Nrf2 pathway in transferred Th2 cells. Consistent with this result, Txnip deficiency resulted in the decreased protein expression of Nrf2. Nrf2, a basic leucine zipper (bZip) transcription factor, controls the cellular antioxidant responses (29). The expression of *Blvrb*, an Nrf2 target gene, as well as the protein level and activity of Blvrb, was down-regulated in *Txnip*-deficient transferred Th2 cells. Our ATAC-Seq results suggest that Txnip regulates the expression of *Blvrb* epigenetically. Thus, our results indicate that Txnip regulates cellular redox metabolism via the epigenetic control of the expression of *Blvrb*.

In our experimental model of allergic airway inflammation, the expression of *Txnip* in allergen-specific memory Th2 cells regulated the pathology of allergic airway inflammation. Both *Txnip*-deficient and *Txnip*-overexpressing memory Th2 cells showed similar levels of cytokine production to control memory Th2 cells. Furthermore, the loss of Txnip showed little effect on the production of effector cytokines, such as IL-4, IL-5, and IL-13, by effector Th2 cells. However, *Txnip* deficiency resulted in an increased amount of cellular ROS and decreased formation of memory Th2 cells in vivo. Thus, ROS metabolic reprogramming by Txnip may regulate the quantity—not the quality—of memory Th2 cells. In any event, targeting redox metabolism in allergen-specific Th2 cells may be a novel therapeutic target for allergen-specific airway inflammation.

In summary, we identified a unique metabolic mechanism that controls the formation of allergen-specific memory Th2 cells. We elucidated the critical role of the Txnip–Nrf2–Blvrb axis in the redox metabolism of CD4<sup>+</sup> T cells for the formation of allergen-specific memory T cells, which induce the pathology of allergic airway inflammation. Understanding the metabolic mechanisms that govern the formation of CD4<sup>+</sup> memory T cells

will be crucial for the development of new therapeutic strategies for intractable inflammatory diseases.

## Materials and Methods

Detailed descriptions of all materials and methods are provided in *SI Appendix, Materials and Methods*. In brief, splenic naïve CD4<sup>+</sup> T cells (CD44<sup>lo</sup>CD62L<sup>hi</sup>) from DO11.10 OVA-specific TCR transgenic mice were transferred intravenously into BALB/c recipient mice. The mice that were transferred naïve CD4<sup>+</sup> T cells were immunized with 100 µg OVA (Sigma-Aldrich) and 4 mg Alum (Thermo Fisher Scientific) administered intraperitoneally on 1 and 6 d after cell transfer. Before the first immunization, KJ1<sup>+</sup>CD62L<sup>hi</sup> T cells in the spleen were purified as naïve CD4<sup>+</sup> T cells. And, 5, 7, 11, 17, 30, and 60 d after cell transfer, KJ1<sup>+</sup>CD44<sup>hi</sup> T cells in the spleen were purified as antigen-recognized T cells. These purified T cells were used to investigate the gene expression and the amount of oxidative stress.

**Data, Materials, and Software Availability.** scRNA-Seq, bulk RNA-Seq and ATAC-Seq datasets data have been deposited in [Genome Expression Omnibus (GEO)] [Accession Number GSE221291 (<https://www.ncbi.nlm.nih.gov/geo/query/acc.cgi?acc=GSE221291>)] (30).

**ACKNOWLEDGMENTS.** We thank K. Sugaya for her excellent technical assistance. We thank A. Matsumoto for providing helpful suggestions. This work was supported by the following grants: Ministry of Education, Culture, Sports, Science and Technology (MEXT Japan) Grants-in-Aid for Scientific Research (Nos. 26221305, JP19H05650, JP20H03685, JP17K08876, JP20KK0351, JP21H05120, JP21H05121, JP21K20754, JP22H02885, and JP22K15484); Practical Research Project for Allergic Diseases and Immunology (Research on Allergic Diseases and Immunology) from the Japan Agency for Medical Research and Development, AMED (Nos. JP19ek0410045, and JP22ek0410092); AMED-CREST, AMED (No. JP22gm1210003); JST FOREST Project (No. JPMJFR200R, Japan); Mochida Memorial Foundation for Medical and Pharmaceutical Research, MSD Life Science Foundation, Takeda Science Foundation, and Kowa Life Science Foundation. K. Kokubo was supported by the PhD Scholarship (Kibou Project) from Japanese Society for Immunology.

Author affiliations: <sup>a</sup>Department of Immunology, Graduate School of Medicine, Chiba University, Chuo-ku, Chiba 260-8670, Japan; <sup>b</sup>Institute for Advanced Academic Research, Chiba University, Chuo-ku, Chiba 260-8670, Japan; and <sup>c</sup>Core Research for Evolutionary Science and Technology, Japan Agency for Medical Research and Development, Chuo-ku, Chiba 260-8670, Japan

- M. Ruterbusch, K. B. Pruner, L. Shehata, M. Pepper, In vivo CD4(+) T cell differentiation and function: Revisiting the Th1/Th2 paradigm. *Annu. Rev. Immunol.* **38**, 705–725 (2020).
- T. Nakayama *et al.*, Th2 cells in health and disease. *Annu. Rev. Immunol.* **35**, 53–84 (2017).
- S. C. Jameson, D. Masopust, Understanding subset diversity in T cell memory. *Immunity* **48**, 214–226 (2018).
- B. Pulendran, R. Ahmed, Immunological mechanisms of vaccination. *Nat. Immunol.* **12**, 509–517 (2011).
- J. T. Chang, E. J. Wherry, A. W. Goldrath, Molecular regulation of effector and memory T cell differentiation. *Nat. Immunol.* **15**, 1104–1115 (2014).
- K. Araki *et al.*, mTOR regulates memory CD8 T-cell differentiation. *Nature* **460**, 108–112 (2009).
- K. N. Pollizzi *et al.*, mTORC1 and mTORC2 selectively regulate CD8(+) T cell differentiation. *J. Clin. Invest.* **125**, 2090–2108 (2015).
- K. Ganeshan, A. Chawla, Metabolic regulation of immune responses. *Annu. Rev. Immunol.* **32**, 609–634 (2014).
- R. I. K. Gellink, R. L. Kyle, E. L. Pearce, Unraveling the complex interplay between T cell metabolism and function. *Annu. Rev. Immunol.* **36**, 461–488 (2018).
- N. M. Chapman, M. R. Boothby, H. Chi, Metabolic coordination of T cell quiescence and activation. *Nat. Rev. Immunol.* **20**, 55–70 (2020).
- N. J. Machver, R. D. Michalek, J. C. Rathmell, Metabolic regulation of T lymphocytes. *Annu. Rev. Immunol.* **31**, 259–283 (2013).
- T. W. Mak *et al.*, Glutathione primes T cell metabolism for inflammation. *Immunity* **46**, 675–689 (2017).
- S. H. Jackson, S. Devadas, J. Kwon, L. A. Pinto, M. S. Williams, T cells express a phagocyte-type NADPH oxidase that is activated after T cell receptor stimulation. *Nat. Immunol.* **5**, 818–827 (2004).
- D. G. Franchina, C. Dostert, D. Brenner, Reactive oxygen species: Involvement in T cell signaling and metabolism. *Trends Immunol.* **39**, 489–502 (2018).
- J. Muri, M. Kopf, Redox regulation of immunometabolism. *Nat. Rev. Immunol.* **21**, 363–381 (2021).
- D. A. Hildeman *et al.*, Reactive oxygen species regulate activation-induced T cell apoptosis. *Immunity* **10**, 735–744 (1999).
- S. Devadas, L. Zaritskaya, S. G. Rhee, L. Oberley, M. S. Williams, Discrete generation of superoxide and hydrogen peroxide by T cell receptor stimulation: Selective regulation of mitogen-activated protein kinase activation and fas ligand expression. *J. Exp. Med.* **195**, 59–70 (2002).
- J. Muri, H. Thut, M. Kopf, The thioredoxin-1 inhibitor Txnip restrains effector T-cell and germinal center B-cell expansion. *Eur. J. Immunol.* **51**, 115–124 (2021).
- A. E. Dikalova *et al.*, Therapeutic targeting of mitochondrial superoxide in hypertension. *Circ. Res.* **107**, 106–116 (2010).
- A. Babahajian *et al.*, Neuroprotective effects of trolox, human chorionic gonadotropin, and carnosic acid on hippocampal neurodegeneration after ischemiareperfusion injury. *Curr. Stem Cell Res. Ther.* **14**, 177–183 (2019).
- R. Franco, W. I. DeHaven, M. I. Sifre, C. D. Bortner, J. A. Cidlowski, Glutathione depletion and disruption of intracellular ionic homeostasis regulate lymphoid cell apoptosis. *J. Biol. Chem.* **283**, 36071–36087 (2008).
- A. Nishiyama *et al.*, Identification of thioredoxin-binding protein-2/vitamin D(3) up-regulated protein 1 as a negative regulator of thioredoxin function and expression. *J. Biol. Chem.* **274**, 21645–21650 (1999).
- J. Hwang *et al.*, The structural basis for the negative regulation of thioredoxin by thioredoxin-interacting protein. *Nat. Commun.* **5**, 2958 (2014).
- H. Sies, C. Berndt, D. P. Jones, Oxidative stress. *Annu. Rev. Biochem.* **86**, 715–748 (2017).
- T. W. Sedlak, S. H. Snyder, Bilirubin benefits: Cellular protection by a biliverdin reductase antioxidant cycle. *Pediatrics* **113**, 1776–1782 (2004).
- L. A. Sena *et al.*, Mitochondria are required for antigen-specific T cell activation through reactive oxygen species signaling. *Immunity* **38**, 225–236 (2013).
- R. I. Klein Gellink *et al.*, Mitochondrial priming by CD28. *Cell* **171**, 385–397.e311 (2017).
- E. Yoshihara *et al.*, Thioredoxin/Txnip: Redoxisome, as a redox switch for the pathogenesis of diseases. *Front. Immunol.* **4**, 514 (2014).
- K. Taguchi, H. Motohashi, M. Yamamoto, Molecular mechanisms of the Keap1-Nrf2 pathway in stress response and cancer evolution. *Genes Cells* **16**, 123–140 (2011).
- M. Kiuchi, Thioredoxin-interacting protein is essential for memory T cell formation via the regulation of the redox metabolism. <https://www.ncbi.nlm.nih.gov/geo/query/acc.cgi?acc=GSE221291>. Deposited 23 December 2022.